Metal-Ion-Modified Black Phosphorus with Enhanced Stability and Transistor Performance

Zhinan Guo, Si Chen, Zhongzheng Wang, Zhenyu Yang, Fei Liu, Yanhua Xu, Jiahong Wang, Ya Yi, Han Zhang, Lei Liao,* Paul K. Chu, and Xue-Feng Yu**

Black phosphorus (BP), a burgeoning elemental 2D semiconductor, has aroused increasing scientific and technological interest, especially as a channel material in field-effect transistors (FETs). However, the intrinsic instability of BP causes practical concern and the transistor performance must also be improved. Here, the use of metal-ion modification to enhance both the stability and transistor performance of BP sheets is described. Ag^+ spontaneously adsorbed on the BP surface via cation–π interactions passivates the lone-pair electrons of P thereby rendering BP more stable in air. Consequently, the Ag^+-modified BP FET shows greatly enhanced hole mobility from 796 to 1666 $cm^2 V^{-1} s^{-1}$ and ON/OFF ratio from 5.9×10^4 to 2.6×10^6. The mechanisms pertaining to the enhanced stability and transistor performance are discussed and the strategy can be extended to other metal ions such as Fe^{3+}, Mg^{2+}, and Hg^{2+}. Such stable and high-performance BP transistors are crucial to electronic and optoelectronic devices. The stability and semiconducting properties of BP sheets can be enhanced tremendously by this novel strategy.

For half a century, silicon (Si) has been used as the semiconductor material to fabricate field-effect transistor (FET) which is now an indispensable building block in almost all electronic products. Today, the physical dimension of transistor is quickly approaching its fundamental scaling limit and further transistor miniaturization is expected to encounter unprecedented challenges.[1] Therefore, the semiconductor industry urgently needs new innovation in materials and devices to replace silicon with a more superior channel material. In recent years, 2D layered materials, such as graphene[1] and transition-metal dichalcogenides (TMDs),[2] have been regarded as hot candidates for FET channel materials due to their specific layered structures and novel physical properties. Although graphene shows extremely high carrier mobility,[3] the lack of a bandgap makes it less favorable for transistor switching.[4] Transistors built on few-layer MoS_2, the most studied TMDs,[5,6] are the optimal forms of ultrathin body FETs with an ideal structure to protect against the short channel effects.[7,8] However, majority of the reported TMD transistors have a much lower carrier mobility performance over graphene or traditional semiconductors.[9,10]

Since 2014, black phosphorus (BP), one of the latest members of 2D layered semiconductors, has been rediscovered from the perspective of 2D materials for transistors with both high carrier mobility and ON/OFF current ratio.[11,12] Different from graphene and TMDs, BP has a thickness-tunable direct bandgap that spans from a bulk value of 0.3 eV to a monolayer value of ≈2.0 eV[13] in addition to highly anisotropic characteristics[14–17] and special optical-response properties.[18–23] Due to these fascinating properties, BP has demonstrated appealing potential for not only building (opto)electronic devices, but also in many other areas such as lithium ion batteries,[24–26] solar cells,[27–29] sensors,[30–35] thermoelectric devices,[36–38] supercapacitors,[39] and phototherapy.[40–43] However, a fundamental obstacle hindering the application of BP is its lack of stability under ambient conditions because BP is very reactive to oxygen and water resulting in rapid degradation of its electronic and optical properties.[44–48] Very recently, some strategies including capping

Dr. Z. Guo, Z. Wang, Dr. J. Wang, Dr. Y. Yi, Prof. X.-F. Yu
Institute of Biomedicine and Biotechnology
Shenzhen Institutes of Advanced Technology
Chinese Academy of Sciences
Shenzhen 518055, P. R. China
E-mail: xf.yu@siat.ac.cn

Dr. Z. Guo, S. Chen, Y. Xu, Prof. H. Zhang
SZU-NUS Collaborative Innovation Center for Optoelectronic Science and Technology, and Key Laboratory of Optoelectronic Devices and Systems of Ministry of Education and Guangdong Province
College of Optoelectronic Engineering
Shenzhen University
Shenzhen 518060, P. R. China
E-mail: hzhang@szu.edu.cn

Z. Wang, Z. Yang, Prof. L. Liao
Department of Physics and Key Laboratory of Artificial Micro- and Nano-structures of Ministry of Education
Wuhan University
Wuhan 430072, P. R. China
E-mail: liaolei@whu.edu.cn

Prof. F. Liu
Department of Physics
The University of Hong Kong
999077 Hong Kong, P. R. China

Prof. P. K. Chu
Department of Physics and Materials Science
City University of Hong Kong
999077 Hong Kong, P. R. China

DOI: 10.1002/adma.201703811

layer protection,[44,48,49] covalent aryl diazonium functionalization,[50] and ligand surface coordination[51] have been suggested to improve the stability of BP. In spite of these progresses, the fabrication of high-performance BP transistors is still very challenging due to the difficulties to simultaneously achieve the stability and high device performance such as carrier mobility and ON/OFF current ratio.

In this paper, a simple metal-ion modification strategy was established to enhance the stability and transistor performance of BP sheets. BP has a well-known puckered honeycomb structure. Within each layer of BP, every phosphorus atom has five outermost orbital electrons, which are three single electrons and one lone pair electrons. Three single electrons were covalently bonded to three other phosphorus atoms and a pair of lone pair electrons is exposed. The lone pair electrons in BP can readily react with oxygen to form P_xO_y[46] and occupation of the lone pair electrons by other elements may prevent the reaction between phosphorus and oxygen ultimately mitigating oxidation of BP.[50,51] Here, metal ions such as Ag^+ were employed to interact with BP forming Ag^+-modified BP (designated as $BP_{Ag(+)}$) to enhance their stability against oxidation and degradation, and in the meanwhile, the enhancement of the transistor performance of the corresponding $BP_{Ag(+)}$ FET was investigated.

The BP sheets are produced by a mechanical exfoliation method with scotch tape from bulk BP as reported previously.[11,12] The BP sheets are transferred to a Si wafer with a 300 nm thick SiO_2 layer through a poly(dimethylsiloxane) (PDMS) thin film as the medium (Figure S1, Supporting Information). The samples are immersed in the *N*-methyl-2-pyrrolidone (NMP) solution containing silver nitrate (1×10^{-6} M) for 2 h, washed with NMP, and dried with argon gas to produce $BP_{Ag(+)}$ sheets on the wafer. NMP is chosen as the solvent because it does not contain water and any chemical groups such as −OH and −COOH which may react with BP.

Scheme 1a illustrates the adsorption mechanism of Ag^+ on BP. In the BP structure, the lone pair electrons of the phosphorus atoms in each layer are evenly distributed on the two sides of the layer and interact with each other forming a conjugated π bond. It is known that metal ions such as Ag^+ can interact with the conjugated π bond via the cation–π interaction.[52] In this case, the relationship between Ag^+ and phosphorus atoms is one to many, rather than one to one. The detailed structure from different views of the $BP_{Ag(+)}$ is shown in Scheme 1b. By conducting density-functional theory (DFT) calculation, the combined energy between silver ions and BP is −41.8 cal suggesting that free Ag^+ can adsorb on the BP surface and the interaction between them is strong enough to obtain stable $BP_{Ag(+)}$.[52]

High-resolution X-ray photoelectron spectroscopy (HR-XPS) is performed to examine adsorption of Ag^+ on BP. $BP_{Ag(+)}$ and bare BP sheets are exposed to air for 3 d before the P 2p and Ag 3d spectra are acquired. As shown in **Figure 1**a, both $BP_{Ag(+)}$ and BP sheets exhibit two peaks at 130.0 eV originating P $2p_{3/2}$ and P $2p_{1/2}$ consistent with previous reports.[48,53] In addition, BP shows a strong peak at 134.0 eV corresponding to the P_xO_y complex indicating serious oxidization of BP during exposure to air.[48,53] However, no P_xO_y peak can be observed from $BP_{Ag(+)}$ indicating better stability against oxidization and the peak at 133.0 eV observed from $BP_{Ag(+)}$ can be attributed to the interaction between Ag^+ and BP. Because the electron withdrawing ability of Ag^+ in $BP_{Ag(+)}$ is much weaker than that of O in P_xO_y, the binding energy of P 2p of P-Ag in $BP_{Ag(+)}$ is 1 eV less than that for P—O in BP. Furthermore, the intensity of the P 2p peak for P—Ag is less than that of elemental P (≈130 eV), indicating that the P—Ag interaction occupies only a small portion of the total P in $BP_{Ag(+)}$, as shown in Figure S2 (Supporting Information). Another direct proof for the successful modification of Ag^+ on $BP_{Ag(+)}$ surface is shown in Figure 1b. Different from the bare BP, a Ag $3d_{5/2}$ peak at 367.8 eV is observed from $BP_{Ag(+)}$ and it is about 0.4 eV less than the standard Ag $3d_{5/2}$ peak of metallic Ag at 368.2 eV. Hence, ionized Ag is attached to BP resulting in a relatively weak interaction (cation–π interaction, which is much less than the covalent binding) with the P atoms on the surface of $BP_{Ag(+)}$. The absence of the loss peaks of Ag (typical Ag metal peaks) from the spectrum of $BP_{Ag(+)}$ also demonstrates that Ag on the $BP_{Ag(+)}$ surface is ionized. Furthermore, the fully XPS measurements on the bare BP and $BP_{Ag(+)}$ are shown in Figure S3 (Supporting Information). The peak intensity of O element in $BP_{Ag(+)}$ is much lower than that in bare BP, confirming its low adsorbability to oxygen.

The Raman scattering spectra acquired from $BP_{Ag(+)}$ and bare BP are displayed in Figure 1c. The three typical BP Raman peaks at 360.9, 438.4, and 466.5 cm^{-1} correspond to the A_g^1, B_{2g}, and A_g^2 vibrational modes of P in BP. With regard to $BP_{Ag(+)}$, the A_g^1 peak is selectively enhanced confirming attachment of Ag^+ on the surface with the enhanced susceptibility tensor of the A_g^1 mode. The results also indicate that the out-of-plane mode (A_g^1) is more sensitive to the surface than in-plane modes (B_{2g} and A_g^2). Figure 1d shows a series of Raman spectra of $BP_{Ag(+)}$ obtained after immersing BP in the Ag^+ NMP solution for different time durations. The intensity of the A_g^1 peak at 360.9 cm^{-1}

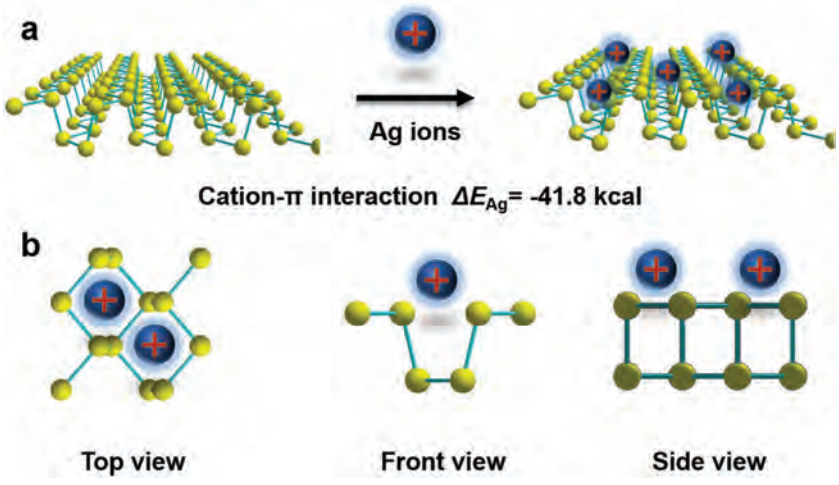

Scheme 1. a) Schematic illustrating adsorption of Ag^+ on BP. b) Three different views of the $BP_{Ag(+)}$ structure.

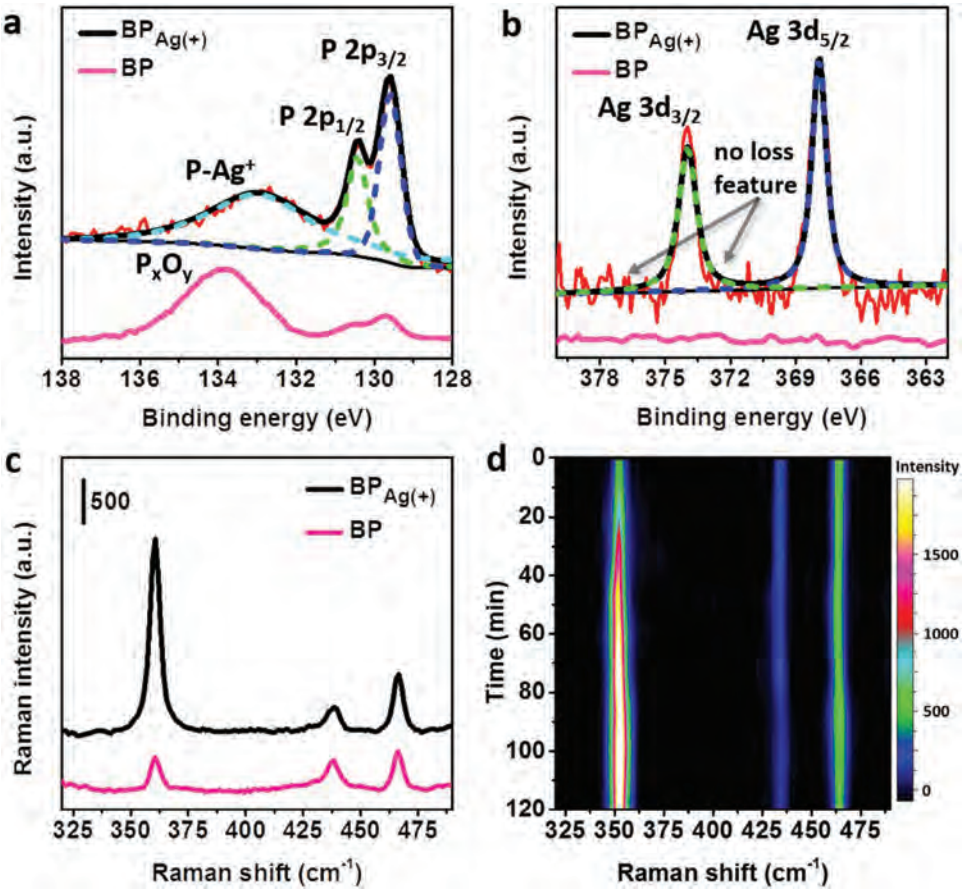

Figure 1. a) HR-XPS spectra of P 2p. b) HR-XPS spectra of Ag 3d. c) Raman spectra of a BP sheet before and after Ag^+ modification. d) Series of Raman spectra of a BP sheet after Ag^+ modification for 0 to 120 min. The intensity scale bar is shown on the right.

is enhanced gradually up to 60 min and then stabilizes due to saturated adsorption of Ag^+ on BP, whereas the intensity of the B_{2g} and A_g^2 peaks are the same, suggesting the Ag^+ modification strategy through cation–π interaction is easy to control. Consequently, an excessive amount of Ag^+ can be used and the reaction ceases spontaneously after the BPs have been fully modified. This scheme is thus more preferable and flexible than other chemical modification methods.

The Raman map on the BP sheet with different layer numbers on different parts is shown in Figure S4a and S3b in the Supporting Information. The intensity of each point in the Raman map agrees well with the thickness of the BP sheet, which can be roughly identified by the color of each part of the BP sheet.[54] The thicker the BP sheet, the higher is the Raman intensity at that location. After the surface of the BP sheet is adsorbed with Ag^+, the Raman intensity of all the points of the sheet increases (see Figure S4c, Supporting Information). Moreover, the intensity at the edge of the sheet is larger than that at the center, suggesting that the edge of the BP sheet has higher binding affinity for Ag^+. The result is consistent with chemical modification in which edge features have been observed after chemical modification for 3 h.[50]

Atomic force microscopy (AFM) is conducted to compare the ambient stability of BP and $BP_{Ag(+)}$, as shown in **Figure 2**. The BP (≈8.2 nm) and $BP_{Ag(+)}$ (≈9.5 nm) sheets on the Si/SiO_2 wafer are kept in air at a relative humidity of 95% and room temperature for 5 d. Both BP and $BP_{Ag(+)}$ show perfectly clean and flat surfaces after the first day. After 2 d, bubbles appear from the bare BP due to the formation of P_xO_y by the reaction with the oxygen and water in air.[44,46,48] After exposure for 5 d, the size of the bubbles increases and some parts of the bare BP sheets vanish. It has been reported that such degradation seriously affects the electronic transport properties thereby hindering its use in electronic devices. In this respect, the surface morphology of $BP_{Ag(+)}$ is preserved and no obvious bubbles, corrosion, or degradation can be observed after 5 d. Figure 2i shows the histogram of the surface roughness of BP and $BP_{Ag(+)}$. It also indicates that only $BP_{Ag(+)}$ can maintain the surface roughness similar to that of the pristine state during exposure to humid air for 5 d. The stability of thinner $BP_{Ag(+)}$ sheet is further tested. As shown in Figure S5 (Supporting Information), the thinner $BP_{Ag(+)}$ sheet (≈3.7 nm) also exhibits good stability as the thicker one. These results demonstrate that the Ag^+ modification can protect BP from degradation for several days in air with a relative humidity as high as 95%. Further experiments find that if the $BP_{Ag(+)}$ products are placed in a drying oven, they can be stable at least for 3 weeks. It should be noted that all the experiments were conducted under room temperature. If the parameters such as temperature and concentration were further optimized, a better stability of the $BP_{Ag(+)}$ could be

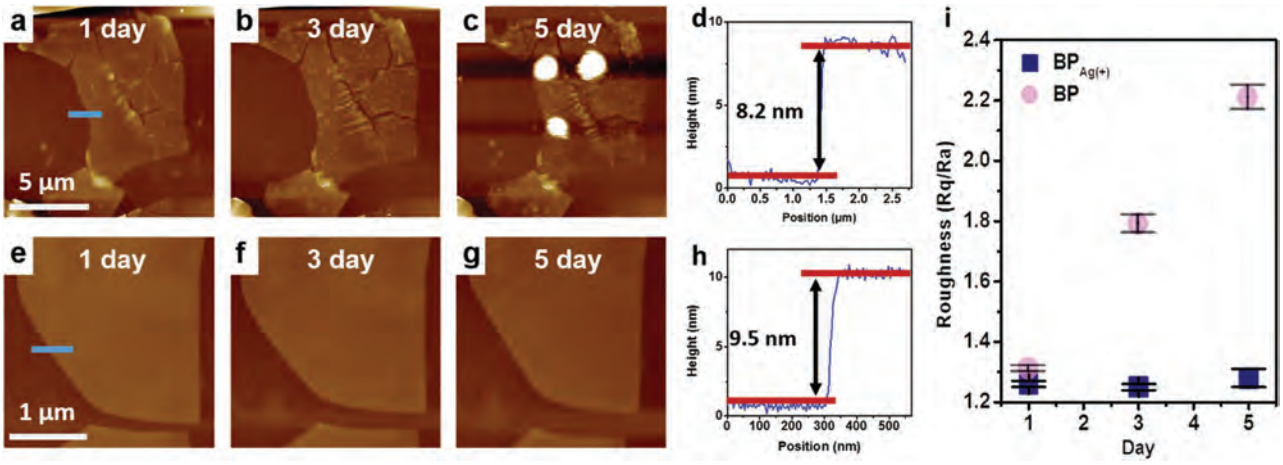

Figure 2. a–d) AFM images of a bare BP sheet exposed to air for 1 d (a), 3 d (b), and 5 d (c), and corresponding height profile (d). e–h) AFM images (e–g) of a $BP_{Ag(+)}$ sheet exposed to air for 1 d (e), 3 d (f), and 5 d (g), and corresponding height profile (h). i) Changes in the surface roughness of the $BP_{Ag(+)}$ and bared BP sheets with exposure time.

obtained. However, the $BP_{Ag(+)}$ here obtained under room temperature exhibits satisfactory stability as a building block for the fabrication of optical and electronic devices.

The BP FET devices are fabricated by traditional micro–nano machining based on electron-beam lithography and the three-electrode system is utilized to assess the transport performance. The typical structure and microscopy image of the few-layer BP FET device are shown in **Figure 3**a. The two electrodes are attached across the BP sheet with a 3 μm channel length for the source and drain electrodes and the other electrode is attached to the Si substrate serving as the backgate electrode. The room-temperature switching behavior of the BP FET before and after

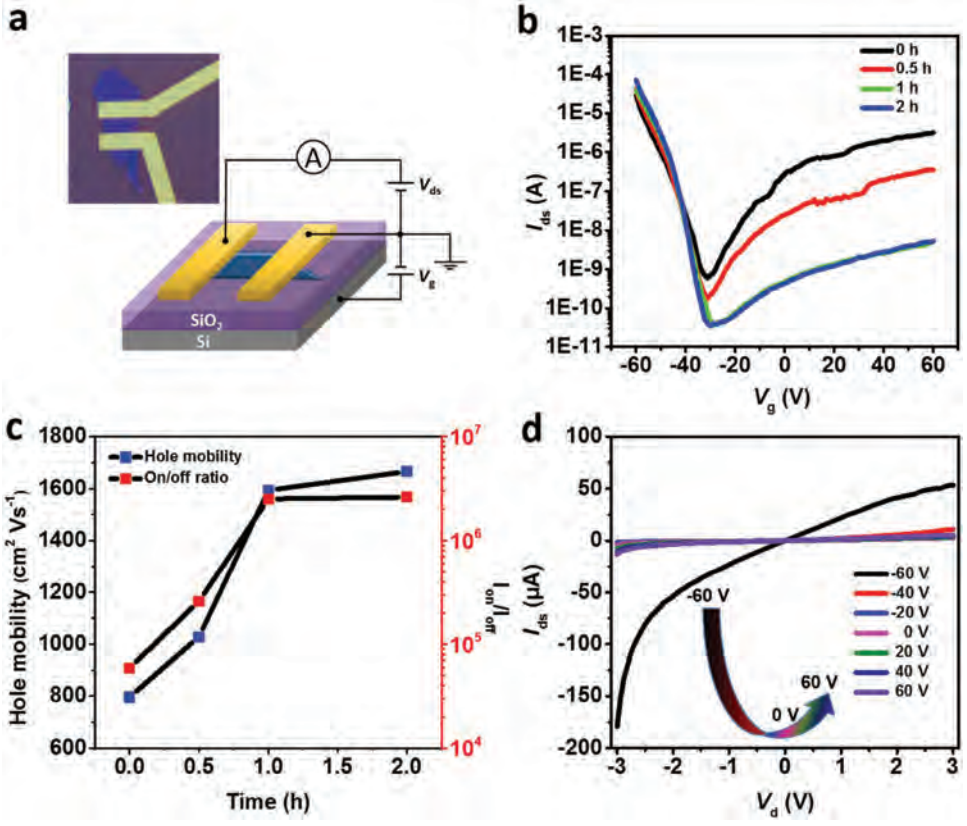

Figure 3. a) Microscopy image (top) and structure schematic of a BP FET device on the silicon substrate with a 300 nm SiO_2. b) Current (logarithmic scale) to gate voltage curve obtained from the BP FET at room temperature after Ag^+ modification for 0, 0.5, 1, and 2 h. c) Hole mobility and ON/OFF ratio of the FET device as a function of Ag^+ modification time. d) Current to bias voltage characteristics at V_g from −60 to 60 V at a step of 20 V for the $BP_{Ag(+)}$ FET after Ag^+ modification for 2 h.

Ag^+ modification is determined in vacuum (1×10^{-5} mbar). By sweeping the backgate voltage V_g on the degenerated doped silicon, the current between the source and drain probed across the BP conductive channel is monitored at a bias V_{ds} of 1 V. The variation in the I_{ds}–V_g curve of the BP FET with Ag^+ modification time is presented in Figure 3b. As the backgate voltage is swept from −60 to 60 V, the channels on the bare BP and $BP_{Ag(+)}$ (modification time of 0.5 h) switch from the "on" state to the "off" state and then to the "on" state again, indicating the ambipolar transport behavior.[55] As the Ag^+ modification time is extended from 0.5 to 2 h, the initial current increases gradually and the "off" state current is smaller, while the current from the "off" state to the right-side "on" state becomes weak. It means that the original ambipolar transport behavior of BP changes to a more p-type transport as Ag^+ gradually adsorbs onto the surface. Figure 3c shows the variation in the hole mobility and ON/OFF ratio of the BP FET after Ag^+ modification. After modification for 1 h, the hole mobility increases from 796 to 1593 $cm^2\ V^{-1}\ s^{-1}$ and the ON/OFF ratio changes from 5.9×10^4 to 2.5×10^6. After modification for 2 h, the hole mobility and ON/OFF ratio increase slightly. Owing to saturated adsorption of Ag^+, the modification process ceases automatically after 1 h consistent with the Raman results. The slightly enhanced performance observed in the second hour during modification can be attributed to the rearrangement process of Ag^+ on the BP surface reaching a more stable state (Figure S6, Supporting Information). To exclude the influence of NMP, control experiments in which BP is treated with NMP without Ag^+ are performed. Figure S7 (Supporting Information) reveals no transport enhancement thereby confirming the effect of Ag^+ on the enhanced device performance. Finally, the hole mobility of the $BP_{Ag(+)}$ FET reaches 1666 $cm^2\ V^{-1}\ s^{-1}$, that is more than 2 times higher than that of the original bare BP device, and the ON/OFF ratio reaches 2.6×10^6, which is 44 times of the original value. Figure 3d and Figure S8 (Supporting Information) show the output behavior of the $BP_{Ag(+)}$ FET after modification for 2 h disclosing a linear relationship between I_{ds} and V_{ds} at low V_{ds} and saturated I_{ds} at high V_{ds}. Although the linear relationship between I_{ds} and V_{ds} indicates good Ohmic contact between the $BP_{Ag(+)}$ and Cr/Au electrodes, Schottky barrier (SB) may still exist because for ultrathin body devices tunneling through SB also results in a linear I–V curve at room temperature.[56] The saturation observed from I_{ds} suggests that carrier transportation can be controlled by the backgate voltage.

The mechanism of the Ag^+ induced hole-transport enhancement of the BP FET is analyzed. It is known that when an electron deficient medium is introduced to an ambipolar transport system, the hole transport part is affected.[57] When Ag^+ is adsorbed on the surface of BP, it brings more holes into the FET device, which in turn enhances the hole transportation and hinders the electron transportation. In order to interpret the mechanism based on the band theory, theoretical simulation based on first-principles calculation is performed with DFT implemented in the Vienna ab initio simulation package. The simulated band structures of the intrinsic monolayer BP and monolayer $BP_{Ag(+)}$ are shown in Figure S9a (Supporting Information). There is no new impurity energy level in the band structures after Ag^+ modification. In this case, the transport behavior in the transistor fabricated on BP and $BP_{Ag(+)}$ can be divided into three stages, namely hole transport, switching point, and electron transport, as shown in Figure S9b (Supporting Information). After Ag^+ is adsorbed onto the surface of BP, it brings in an electron deficient medium. It elevates both of the valence band (E_v) and conduction band (E_c) of BP and in turn, induces a relatively lower metal Fermi level (E_f) in the metal–semiconductor system of BP and electrodes. The relatively lower metal Fermi level results in a weak energy barrier for tunneling of carriers in the hole transport stage and a strong energy barrier in the electron transport stage. Therefore, Ag^+ modification enhances the initial current of the hole-transport side, lowers the off-state current, enhances the ON/OFF current ratio, and suppresses the electron transport behavior.

The stability of the $BP_{Ag(+)}$ FET is further examined by exposure to air with a relative humidity of 95% at room temperature. The transport properties of the device are determined every 12 h. As shown in **Figure 4**a and Figure S10 (Supporting Information), the transport properties of the $BP_{Ag(+)}$ device are maintained in the first 60 h and only a slight decline is observed in the sixth 12 h. By contrast, the transport properties of the FET

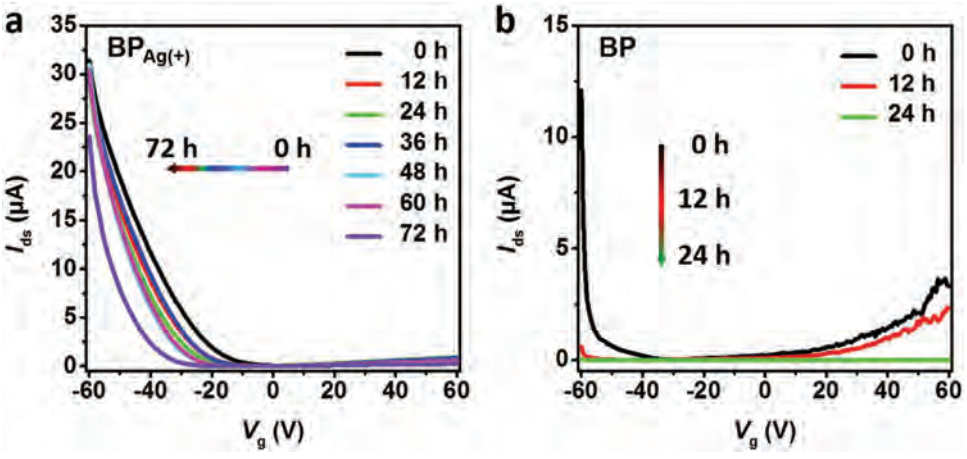

Figure 4. a) Current to gate voltage curve obtained from a $BP_{Ag(+)}$ FET device after air exposure for 0–72 h. b) Current to gate voltage curve obtained from a BP FET device after air exposure for 0–24 h for comparison.

device fabricated on bare BP decline significantly during the first 12 h and the device becomes nonconducting after 24 h, as shown in Figure 4b. The decline in the transport properties of the device stems from oxidization of BP in an atmosphere containing O_2 and H_2O. For the $BP_{Ag(+)}$ device, owing to the protection rendered by Ag^+, the transport performance is preserved for nearly 3 d in air with a humidity as high as 95%. Furthermore, a two-cycle transport-behavior-monitoring experiment is preformed to test the stability of the $BP_{Ag(+)}$ FET device at different temperatures. As shown in Figure S11 (Supporting Information), the stability of the $BP_{Ag(+)}$ FET device can be preserved when the temperature is changed from 298 K (room temperature) to 253 K and 323 K, although its transport behavior is changed with the temperature.

The possible effects of other metal ions on the stability and transistor properties of BP are investigated. The combined energy between BP and commonly used metal ions is calculated by DFT simulation (see Figure S12, Supporting Information). Although the binding energies are different, they are all negative demonstrating the possibility of spontaneous adsorption on the BP surface through cation–π interaction.[52] However, not all salts containing the desired metal can be dissolved in NMP to produce free metal ions. Our solubility test reveals that four salts containing Ag^+, Mg^{2+}, Fe^{3+}, and Hg^{2+}, respectively, have good solubility in NMP. Based on the aforementioned detailed investigation on Ag^+, the influence of the three metal ions, namely Mg^{2+}, Fe^{3+}, and Hg^{2+}, is studied further. The XPS results in Figure S13 (Supporting Information) illustrate successful adsorption of these three metal ions on the BP surface. The AFM images in Figure S14 (Supporting Information) show $BP_{Mg(2+)}$, $BP_{Fe(3+)}$, and $BP_{Hg(2+)}$ sheets after exposure to air with a humidity of 95% for different time durations. Like Ag^+, all three metal ions enhance the stability of BP and the BP sheets after modification is stable for at least 3 d in moist air. The influences of these metal ions on the transport properties of BP FETs were also investigated (see Figure S15, Supporting Information). Like Ag^+, all the three metal ions play electron deficient medium roles in the BP FETs. In particular, after modification for 2 h with Fe^{3+}, the original ambipolar transport behavior of BP changes to a p-type one probably due to the more positive charges of Fe^{3+}. Nonetheless, although all three metal ions improve the transport performance of BP FETs, the performance rendered by Ag^+ is the best.

In conclusion, metal-ion modification is implemented to enhance the stability and transistor performance of BP. The free Ag^+ adsorbs spontaneously on the BP surface by cation–π interaction to passivate the lone-pair electrons of the P atoms to make BP more stable in air. The Ag^+-modified BP FET shows hole mobility of 1666 $cm^2\ V^{-1}\ s^{-1}$ that is more than 2 times higher than that of bare BP and ON/OFF ratio to 2.6×10^6 which is 44 times higher than that of bare BP. Compared to other surface modification strategies, the ion concentration and modification time can be controlled and this methodology can be extended to other metal ions such as Fe^{3+}, Mg^{2+}, and Hg^{2+}. Our results suggest a simple and effective means to enhance both the stability and transistor performance of BP and the stable BP FET described here has large potential in electronic and optoelectronic devices.

Experimental Section

Materials: The BP crystals were purchased from Smart-Elements and stored in a dark Ar glovebox. NMP (99.5%, anhydrous) was obtained from Aladdin Reagents and silver nitrate was purchased from Sigma-Aldrich (Santa Barbara, CA, USA). The chemicals used in this study were analytical reagent grade and used without further purification.

Metal-Ion Modification of BP Sheets: The few-layer BP sheets were prepared by mechanical exfoliation of bulk BP with scotch tape and transferred to a Si/SiO_2 (300 nm) wafer with a PDMS thin film as the medium. The wafer with attached BP sheets were immersed in the NMP solution containing the metal ions for different time durations. Afterward, the wafer was taken out, washed with pure NMP, and dried with N_2.

Characterization: XPS was conducted on the Thermo Fisher ESCALAB 250Xi XPS with an Al K_α X-ray source. The sampling depth was less than 10 nm. The XPS peaks were calibrated by the standard C 1s peak at 284.8 eV according to the Thermo SCIENTIFIC XPS Knowledge Base. Raman scattering was performed on the Horiba Jobin–Yvon LabRam HR-VIS high-resolution confocal Raman microscope equipped with a 633 nm laser as the excitation source at room temperature and a XYZ motorized sample stage controlled by LabSpec software. A 50× objective lens with a numerical aperture of 0. 90 was used to reduce the spot size of the 633 nm laser to about 1 μm. AFM was performed on the Bruker Dimension Icon AFM system in the standard tapping mode. To minimize sample degradation in air, AFM was carried out immediately after the samples were prepared. The BP sheets on the Si/SiO_2 (300 nm) wafer were spin-coated with methyl methacrylate (MMA) and poly(methyl methacrylate) (PMMA) and electron-beam lithography (JEOL 6510 with NPGS system) was employed to define the drain and source patterns. The Cr/Au (15 nm/50 nm) electrodes were fabricated by metal evaporation and the lift-off process. The BP FETs were evaluated on the Lake Shore TTPX Probe Station in vacuum (1×10^{-5} mbar) as well as Keithley 4200 semiconductor characterization system.

Carrier Mobility Calculation: The carrier mobility was extracted from the gating characteristics I_{ds}–I_{gs} at constant V_{ds} = 1 V as shown in Figure 3b according to the following equation:

$$\mu = \frac{1}{C_i}\frac{L}{W}\frac{dI_{ds}}{dV_{gs}}\frac{1}{V_{ds}} \quad (1)$$

where C_i is the capacitance per unit area between the conducting channel and the back gate ($C_i = \varepsilon_0\varepsilon_r/d$; ε_r = 3.9 for SiO_2; d is the thickness of insulating layer SiO_2, 300 nm), L is the channel length (≈3 μm), and W is the channel width (1–3 μm for different devices).

Supporting Information

Supporting Information is available from the Wiley Online Library or from the author.

Acknowledgements

The authors acknowledge financial support from the National Natural Science Foundation of China (Grant Nos. 51672305, 61605131, and 61435010), Frontier Research Key Project of the Chinese Academy of Sciences Grant No. QYZDB-SSW-SLH034, Shenzhen Science and Technology Research Funding Nos. JCYJ20150324141711624, JCYJ20160229195124187, and KQTD2015032416270385, Science and Technology Innovation Commission of Shenzhen Grant Nos. KQTD2015032416270385 and JCYJ20150625103619275, and City University of Hong Kong Strategic Research Grant (SRG) No. 7004644.

Conflict of Interest

The authors declare no conflict of interest.

Keywords

2D materials, black phosphorus, Raman, transistors

Received: July 9, 2017
Revised: August 14, 2017
Published online: September 28, 2017

[1] K. S. Novoselov, A. K. Geim, S. V. Morozov, D. Jiang, Y. Zhang, S. V. Dubonos, I. V. Grigorieva, A. A. Firsov, *Science* **2004**, *306*, 666.
[2] Q. H. Wang, K. Kalantar-Zadeh, A. Kis, J. N. Coleman, M. S. Strano, *Nat. Nano* **2012**, *7*, 699.
[3] K. I. Bolotin, K. J. Sikes, Z. Jiang, M. Klima, G. Fudenberg, J. Hone, P. Kim, H. L. Stormer, *Solid State Commun.* **2008**, *146*, 351.
[4] L. Liao, Y.-C. Lin, M. Bao, R. Cheng, J. Bai, Y. Liu, Y. Qu, K. L. Wang, Y. Huang, X. Duan, *Nature* **2010**, *467*, 305.
[5] L. M. Zhang, K. H. Liu, A. B. Wong, J. Kim, X. P. Hong, C. Liu, T. Cao, S. G. Louie, F. Wang, P. D. Yang, *Nano Lett.* **2014**, *14*, 6418.
[6] K. H. Liu, L. M. Zhang, T. Cao, C. H. Jin, D. A. Qiu, Q. Zhou, A. Zettl, P. D. Yang, S. G. Louie, F. Wang, *Nat. Commun.* **2014**, *5*, 6.
[7] B. Radisavljevic, A. Radenovic, J. Brivio, V. Giacometti, A. Kis, *Nat. Nanotechnol.* **2011**, *6*, 147.
[8] K. F. Mak, C. Lee, J. Hone, J. Shan, T. F. Heinz, *Phys. Rev. Lett.* **2010**, *105*, 4.
[9] M. S. Xu, T. Liang, M. M. Shi, H. Z. Chen, *Chem. Rev.* **2013**, *113*, 3766.
[10] S. Z. Butler, S. M. Hollen, L. Y. Cao, Y. Cui, J. A. Gupta, H. R. Gutierrez, T. F. Heinz, S. S. Hong, J. X. Huang, A. F. Ismach, E. Johnston-Halperin, M. Kuno, V. V. Plashnitsa, R. D. Robinson, R. S. Ruoff, S. Salahuddin, J. Shan, L. Shi, M. G. Spencer, M. Terrones, W. Windl, J. E. Goldberger, *ACS Nano* **2013**, *7*, 2898.
[11] L. K. Li, Y. J. Yu, G. J. Ye, Q. Q. Ge, X. D. Ou, H. Wu, D. L. Feng, X. H. Chen, Y. B. Zhang, *Nat. Nanotechnol.* **2014**, *9*, 372.
[12] H. Liu, A. T. Neal, Z. Zhu, Z. Luo, X. F. Xu, D. Tomanek, P. D. Ye, *ACS Nano* **2014**, *8*, 4033.
[13] H. Liu, Y. C. Du, Y. X. Deng, P. D. Ye, *Chem. Soc. Rev.* **2015**, *44*, 2732.
[14] J. X. Wu, N. N. Mao, L. M. Xie, H. Xu, J. Zhang, *Angew. Chem., Int. Ed.* **2015**, *54*, 2366.
[15] B. Smith, B. Vermeersch, J. Carrete, E. Ou, J. Kim, N. Mingo, D. Akinwande, L. Shi, *Adv. Mater.* **2017**, *29*, 1603756.
[16] J. S. Qiao, X. H. Kong, Z. X. Hu, F. Yang, W. Ji, *Nat. Commun.* **2014**, *5*, 7.
[17] F. N. Xia, H. Wang, Y. C. Jia, *Nat. Commun.* **2014**, *5*, 6.
[18] S. B. Lu, L. L. Miao, Z. N. Guo, X. Qi, C. J. Zhao, H. Zhang, S. C. Wen, D. Y. Tang, D. Y. Fan, *Opt. Express* **2015**, *23*, 11183.
[19] Y. Chen, G. B. Jiang, S. Q. Chen, Z. N. Guo, X. F. Yu, C. J. Zhao, H. Zhang, Q. L. Bao, S. C. Wen, D. Y. Tang, D. Y. Fan, *Opt. Express* **2015**, *23*, 12823.
[20] S. Zhang, J. Yang, R. J. Xu, F. Wang, W. F. Li, M. Ghufran, Y. W. Zhang, Z. F. Yu, G. Zhang, Q. H. Qin, Y. R. Lu, *ACS Nano* **2014**, *8*, 9590.
[21] D. Hanlon, C. Backes, E. Doherty, C. S. Cucinotta, N. C. Berner, C. Boland, K. Lee, A. Harvey, P. Lynch, Z. Gholamvand, S. F. Zhang, K. P. Wang, G. Moynihan, A. Pokle, Q. M. Ramasse, N. McEvoy, W. J. Blau, J. Wang, G. Abellan, F. Hauke, A. Hirsch, S. Sanvito, D. D. O'Regan, G. S. Duesberg, V. Nicolosi, J. N. Coleman, *Nat. Commun.* **2015**, *6*, 11.
[22] T. Low, A. S. Rodin, A. Carvalho, Y. J. Jiang, H. Wang, F. N. Xia, A. H. C. Neto, *Phys. Rev. B* **2014**, *90*, 5.
[23] Z. N. Guo, H. Zhang, S. B. Lu, Z. T. Wang, S. Y. Tang, J. D. Shao, Z. B. Sun, H. H. Xie, H. Y. Wang, X. F. Yu, P. K. Chu, *Adv. Funct. Mater.* **2015**, *25*, 6996.
[24] C. M. Park, H. J. Sohn, *Adv. Mater.* **2007**, *19*, 2465.
[25] J. Sun, G. Y. Zheng, H. W. Lee, N. Liu, H. T. Wang, H. B. Yao, W. S. Yang, Y. Cui, *Nano Lett.* **2014**, *14*, 4573.
[26] W. F. Li, Y. M. Yang, G. Zhang, Y. W. Zhang, *Nano Lett.* **2015**, *15*, 1691.
[27] J. Dai, X. C. Zeng, *J. Phys. Chem. Lett.* **2014**, *5*, 1289.
[28] M. Buscema, D. J. Groenendijk, G. A. Steele, H. S. J. van der Zant, A. Castellanos-Gomez, *Nat. Commun.* **2014**, *5*, 6.
[29] W. Hu, L. Lin, C. Yang, J. Dai, J. L. Yang, *Nano Lett.* **2016**, *16*, 1675.
[30] S. M. Cui, H. H. Pu, S. A. Wells, Z. H. Wen, S. Mao, J. B. Chang, M. C. Hersam, J. H. Chen, *Nat. Commun.* **2015**, *6*, 9.
[31] L. Z. Kou, T. Frauenheim, C. F. Chen, *J. Phys. Chem. Lett.* **2014**, *5*, 2675.
[32] C. C. Mayorga-Martinez, Z. Sofer, M. Pumera, *Angew. Chem., Int. Ed.* **2015**, *54*, 14317.
[33] H. T. Yuan, X. G. Liu, F. Afshinmanesh, W. Li, G. Xu, J. Sun, B. Lian, A. G. Curto, G. J. Ye, Y. Hikita, Z. X. Shen, S. C. Zhang, X. H. Chen, M. Brongersma, H. Y. Hwang, Y. Cui, *Nat. Nanotechnol.* **2015**, *10*, 707.
[34] N. Youngblood, C. Chen, S. J. Koester, M. Li, *Nat. Photonics* **2015**, *9*, 247.
[35] L. Viti, J. Hu, D. Coquillat, W. Knap, A. Tredicucci, A. Politano, M. S. Vitiello, *Adv. Mater.* **2015**, *27*, 5567.
[36] S. Lee, F. Yang, J. Suh, S. J. Yang, Y. Lee, G. Li, H. S. Choe, A. Suslu, Y. B. Chen, C. Ko, J. Park, K. Liu, J. B. Li, K. Hippalgaonkar, J. J. Urban, S. Tongay, J. Q. Wu, *Nat. Commun.* **2015**, *6*, 7.
[37] S. J. Choi, B. K. Kim, T. H. Lee, Y. H. Kim, Z. Y. Li, E. Pop, J. J. Kim, J. H. Song, M. H. Bae, *Nano Lett.* **2016**, *16*, 3969.
[38] H. J. Jang, J. D. Wood, C. R. Ryder, M. C. Hersam, D. G. Cahill, *Adv. Mater.* **2015**, *27*, 8017.
[39] C. X. Hao, B. C. Yang, F. S. Wen, J. Y. Xiang, L. Li, W. H. Wang, Z. M. Zeng, B. Xu, Z. S. Zhao, Z. Y. Liu, Y. J. Tian, *Adv. Mater.* **2016**, *28*, 3194.
[40] J. D. Shao, H. H. Xie, H. Huang, Z. B. Li, Z. B. Sun, Y. H. Xu, Q. L. Xiao, X. F. Yu, Y. T. Zhao, H. Zhang, H. Y. Wang, P. K. Chu, *Nat. Commun.* **2016**, *7*, 13.
[41] Z. B. Sun, H. H. Xie, S. Y. Tang, X. F. Yu, Z. N. Guo, J. D. Shao, H. Zhang, H. Huang, H. Y. Wang, P. K. Chu, *Angew. Chem., Int. Ed.* **2015**, *54*, 11526.
[42] W. Tao, X. B. Zhu, X. H. Yu, X. W. Zeng, Q. L. Xiao, X. D. Zhang, X. Y. Ji, X. S. Wang, J. J. Shi, H. Zhang, L. Mei, *Adv. Mater.* **2017**, *29*, 10.
[43] W. Chen, J. Ouyang, H. Liu, M. Chen, K. Zeng, J. Sheng, Z. Liu, Y. Han, L. Wang, J. Li, L. Deng, Y.-N. Liu, S. Guo, *Adv. Mater.* **2017**, *29*, 1603864.
[44] R. A. Doganov, E. C. T. O'Farrell, S. P. Koenig, Y. T. Yeo, A. Ziletti, A. Carvalho, D. K. Campbell, D. F. Coker, K. Watanabe, T. Taniguchi, A. H. C. Neto, B. Ozyilmaz, *Nat. Commun.* **2015**, *6*, 7.
[45] M. Buscema, D. J. Groenendijk, S. I. Blanter, G. A. Steele, H. S. J. van der Zant, A. Castellanos-Gomez, *Nano Lett.* **2014**, *14*, 3347.
[46] A. Favron, E. Gaufres, F. Fossard, A. L. Phaneuf-L'Heureux, N. Y. W. Tang, P. L. Levesque, A. Loiseau, R. Leonelli, S. Francoeur, R. Martel, *Nat. Mater.* **2015**, *14*, 826.
[47] A. Avsar, I. J. Vera-Marun, J. Y. Tan, K. Watanabe, T. Taniguchi, A. H. C. Neto, B. Ozyilmaz, *ACS Nano* **2015**, *9*, 4138.
[48] J. D. Wood, S. A. Wells, D. Jariwala, K.-S. Chen, E. Cho, V. K. Sangwan, X. Liu, L. J. Lauhon, T. J. Marks, M. C. Hersam, *Nano Lett.* **2014**, *14*, 6964.

[49] B. S. Wan, B. C. Yang, Y. Wang, J. Y. Zhang, Z. M. Zeng, Z. Y. Liu, W. H. Wang, *Nanotechnology* **2015**, *26*, 6.
[50] C. R. Ryder, J. D. Wood, S. A. Wells, Y. Yang, D. Jariwala, T. J. Marks, G. C. Schatz, M. C. Hersam, *Nat. Chem.* **2016**, *8*, 598.
[51] Y. T. Zhao, H. Y. Wang, H. Huang, Q. L. Xiao, Y. H. Xu, Z. N. Guo, H. H. Xie, J. D. Shao, Z. B. Sun, W. J. Han, X. F. Yu, P. H. Li, P. K. Chu, *Angew. Chem., Int. Ed.* **2016**, *55*, 5003.
[52] J. C. Ma, D. A. Dougherty, *Chem. Rev.* **1997**, *97*, 1303.
[53] J. Kang, J. D. Wood, S. A. Wells, J. H. Lee, X. L. Liu, K. S. Chen, M. C. Hersam, *ACS Nano* **2015**, *9*, 3596.
[54] H. Chen, W. Fei, J. Zhou, C. Miao, W. Guo, *Small* **2017**, *13*, 1602336.
[55] S. Das, M. Demarteau, A. Roelofs, *ACS Nano* **2014**, *8*, 11730.
[56] S. Das, W. Zhang, M. Demarteau, A. Hoffmann, M. Dubey, A. Roelofs, *Nano Lett.* **2014**, *14*, 5733.
[57] S. M. Sze, *Semiconductor Devices: Physics and Technology*, John Wiley & Sons, New York **2002**.

ADVANCED MATERIALS

Supporting Information

for *Adv. Mater.*, DOI: 10.1002/adma.201703811

Metal-Ion-Modified Black Phosphorus with Enhanced Stability and Transistor Performance

Zhinan Guo, Si Chen, Zhongzheng Wang, Zhenyu Yang, Fei Liu, Yanhua Xu, Jiahong Wang, Ya Yi, Han Zhang, Lei Liao,* Paul K. Chu, and Xue-Feng Yu**

Supporting Information

Metal-ion-modified black phosphorus with enhanced stability and transistor performance

Zhinan Guo, Si Chen, Zhongzheng Wang, Zhenyu Yang, Fei Liu, Yanhua Xu, Jiahong Wang, Ya Yi, Han Zhang, Lei Liao*, Paul K. Chu, and Xue-Feng Yu**

Dr Z. Guo, Z. Wang, Dr. J. Wang, Dr. Y. Yi, Prof. X.-F. Yu

Institute of Biomedicine and Biotechnology, Shenzhen Institutes of Advanced Technology, Chinese Academy of Sciences, Shenzhen, 518055, P. R. China. E-mail: xf.yu@siat.ac.cn

Dr. Z. Guo, S. Chen, Y. Xu, Prof. H. Zhang

SZU-NUS Collaborative Innovation Center for Optoelectronic Science and Technology, and Key Laboratory of Optoelectronic Devices and Systems of Ministry of Education and Guangdong Province, College of Optoelectronic Engineering, Shenzhen University, Shenzhen, 518060, P. R. China. E-mail: hzhang@szu.edu.cn

Z. Wang, Z. Yang, Prof. L. Liao

Department of Physics and Key Laboratory of Artificial Micro- and Nano-structures of Ministry of Education, Wuhan University, Wuhan, 430072, P. R. China. E-mail: liaolei@whu.edu.cn

Prof. P. K. Chu

Department of Physics and Materials Science, City University of Hong Kong, Hong Kong, P.R. China.

Prof. F. Liu

Department of Physics, The University of Hong Kong, Hong Kong, P. R. China.

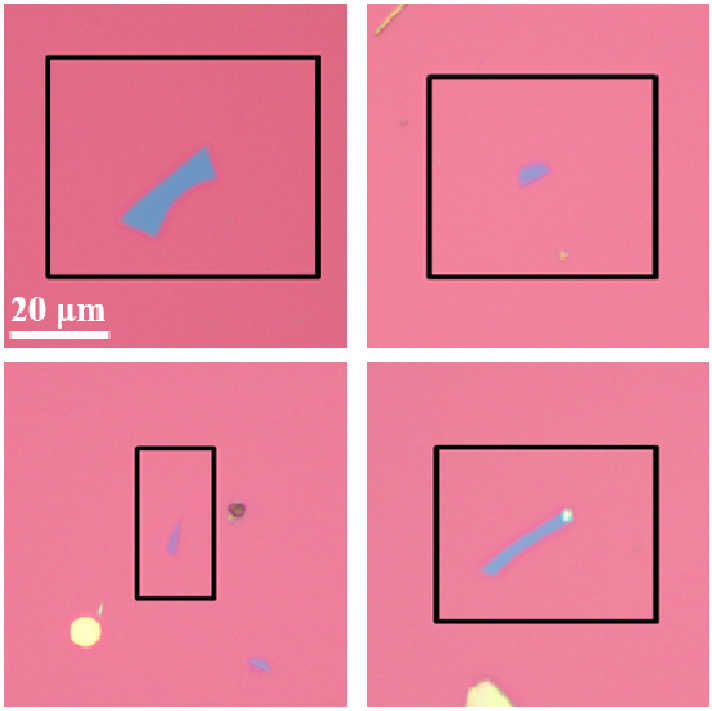

Figure S1. Microphotographs of typical BP sheets on the surface of the Si/SiO_2 (300 nm) wafer.

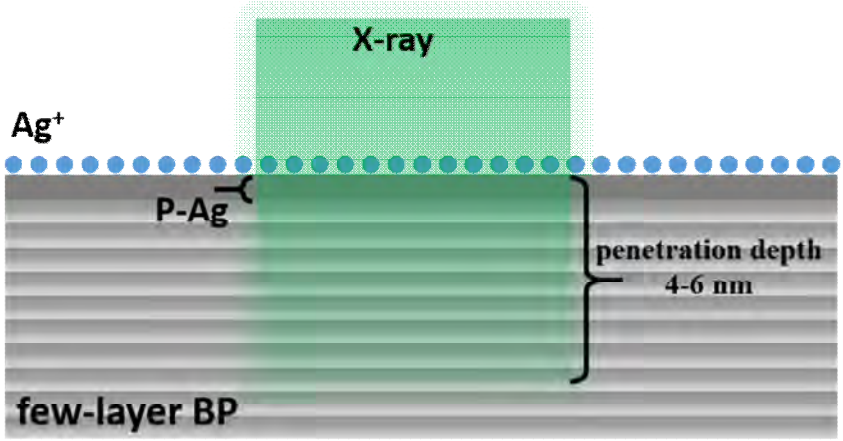

Figure S2. Schematic of the XPS measurement area on a $BP_{Ag(+)}$ sample.

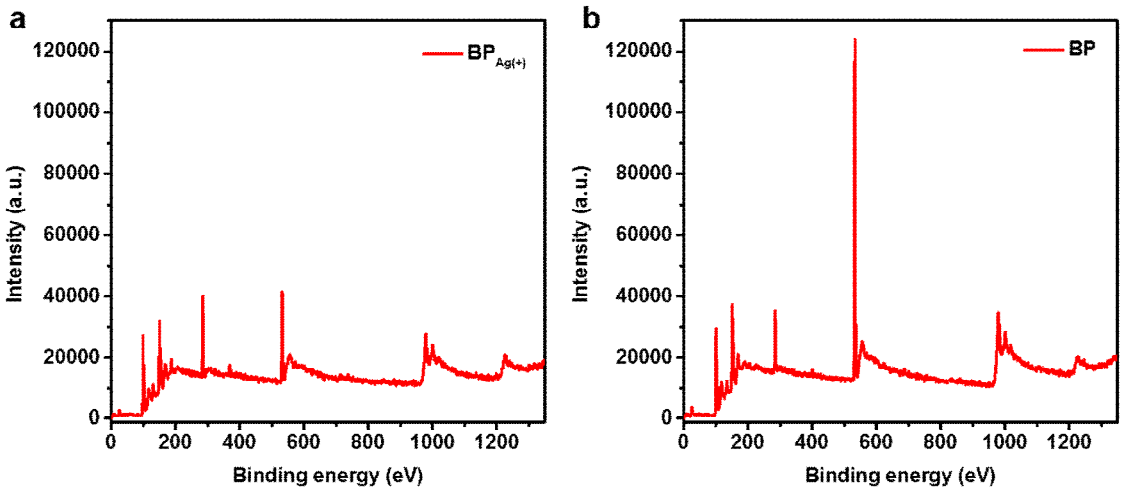

Figure S3. XPS spectra of (a) $BP_{Ag(+)}$ and (b) bare BP sheets after exposure to air for 3 days. The sharp peak at 532 in both spectra arises from O and the intensity of the O peak in (b) is larger than that in (a), indicating that there is more O in the bare BP sample than $BP_{Ag(+)}$.

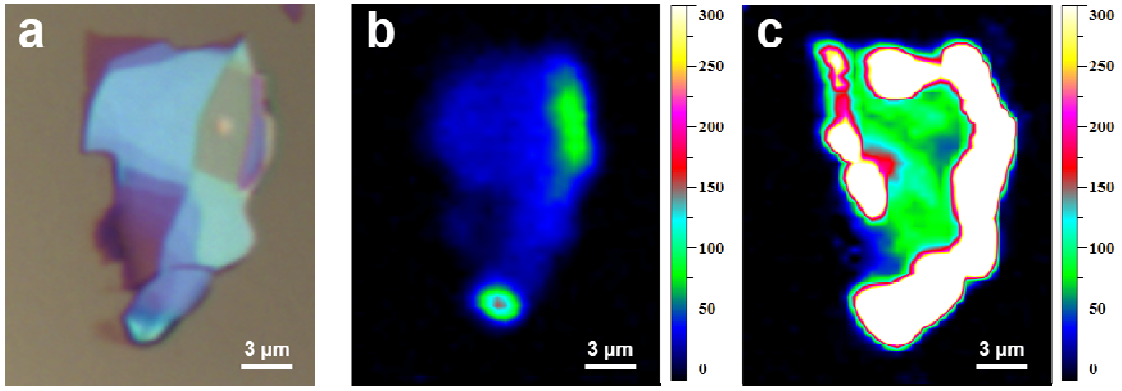

Figure S4 (a) Micrograph of a BP sheet and (b, c) Raman mapping images of the same BP sheet before (b) and after (c) Ag^{+} modification based on the Raman peak of 360.9 cm^{-1}.

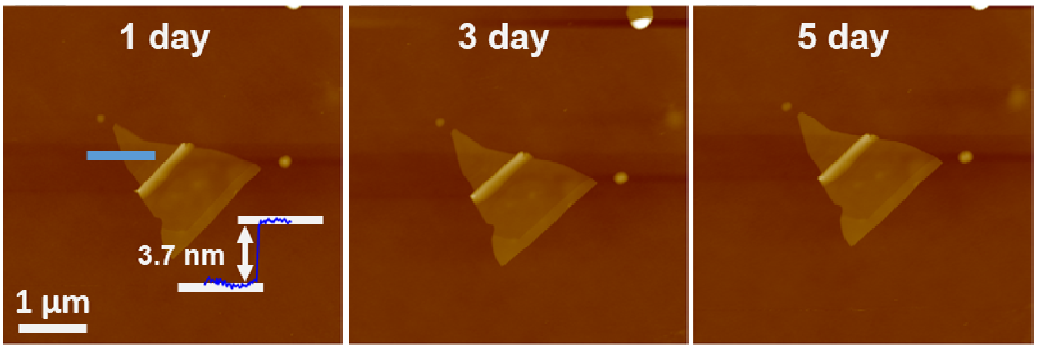

Figure S5. AFM images of a 3.7 nm $BP_{Ag(+)}$ sheet exposed to air for 1 day, 3 days, and 5 days.

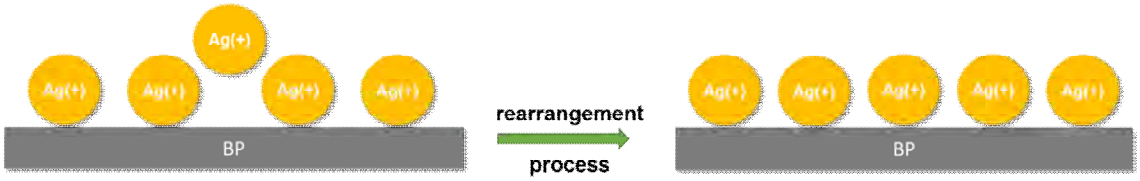

Figure S6. Schematic showing the rearrangement of metal ions on the surface of BP.

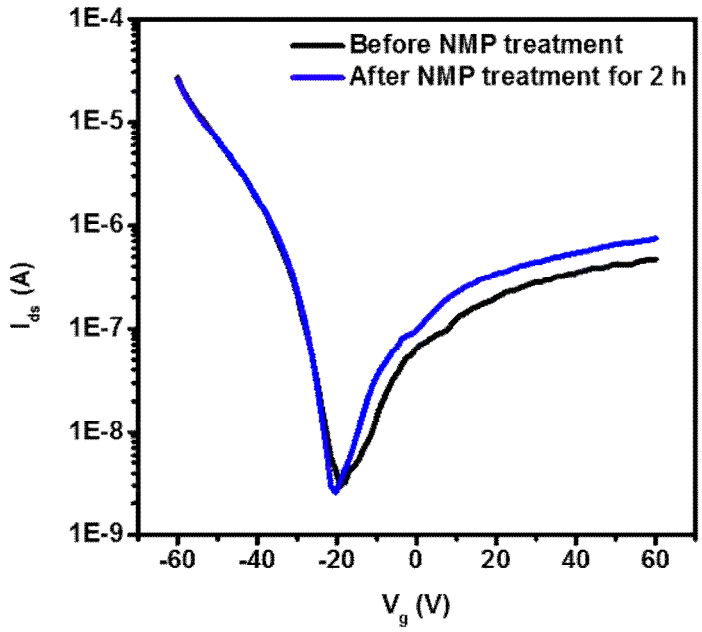

Figure S7. Current (logarithmic scale) to gate voltage curve obtained from the BP FET device on a silicon substrate with a 300 nm thick SiO_2 at room temperature and the same measurement of the device after treatment with pure NMP for 2 h.

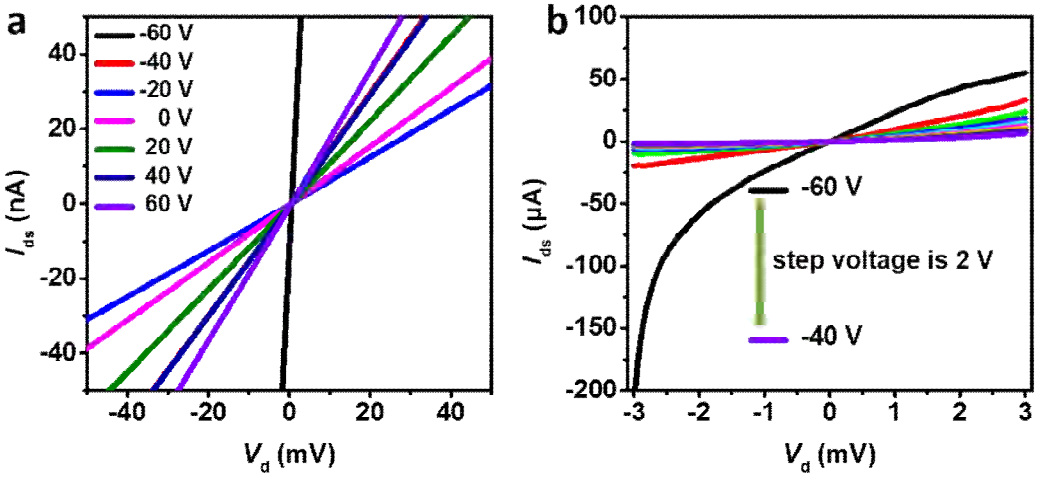

Figure S8. (a) Partial output behavior of the $BP_{Ag(+)}$ device at V_g from -60 to 60 V at a step of 20 V and (b) full output behavior of the $BP_{Ag(+)}$ device at V_g from -60 to -40 V at a step of 2 V.

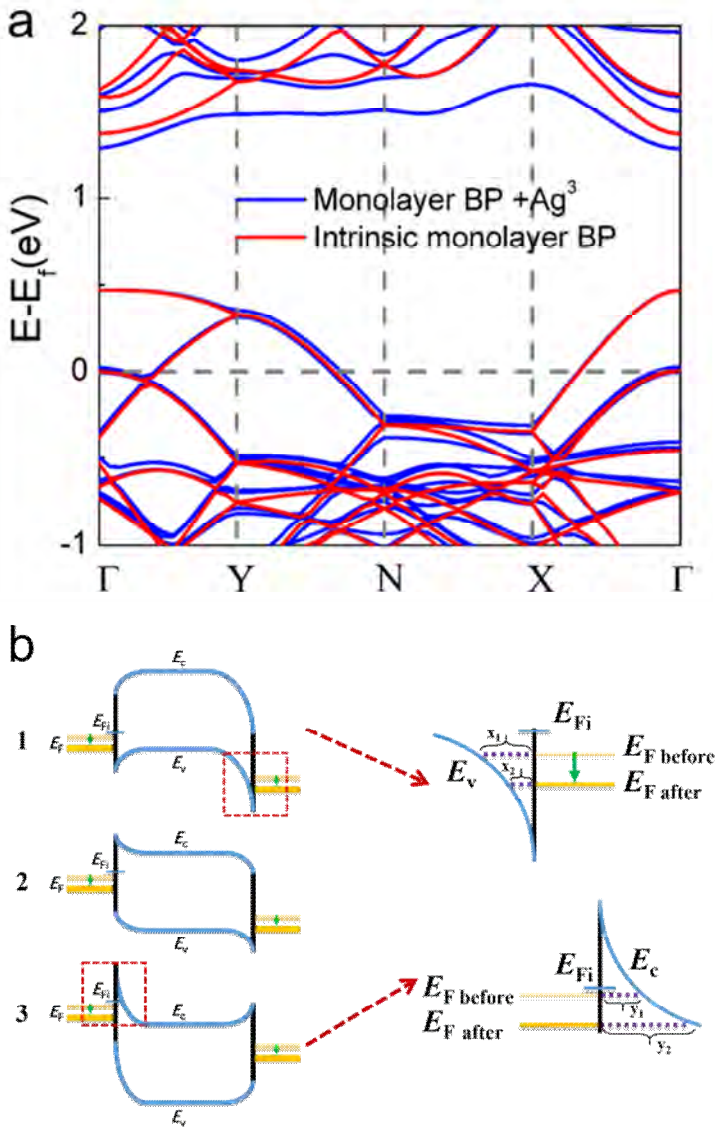

Figure S9. (a) Simulated band structure of the Ag^+-modified monolayer BP with E_f being the Fermi level of the system; (b) Schematic showing the evolution of the contact energy-level diagram of $BP_{Ag(+)}$ and electrode.

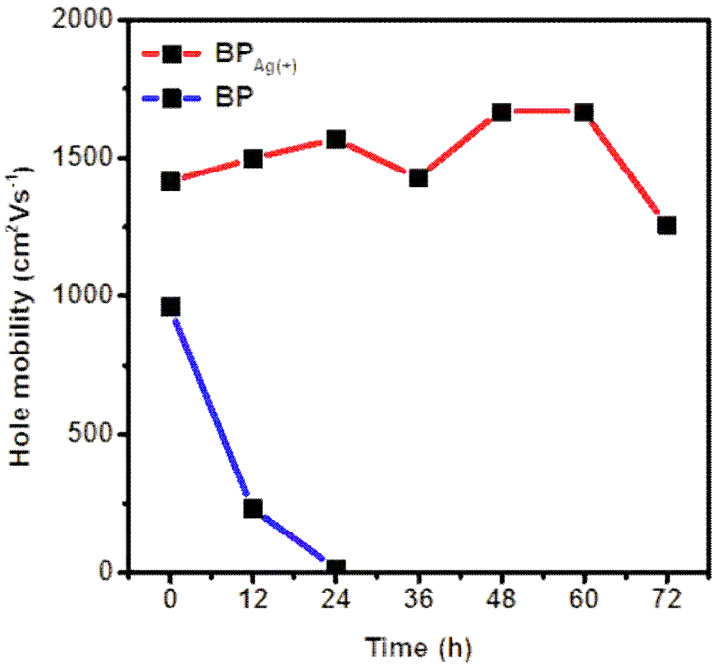

Figure S10. The plot of hole mobility of the FET devices built on $BP_{Ag(+)}$ and BP as a function of exposure time.

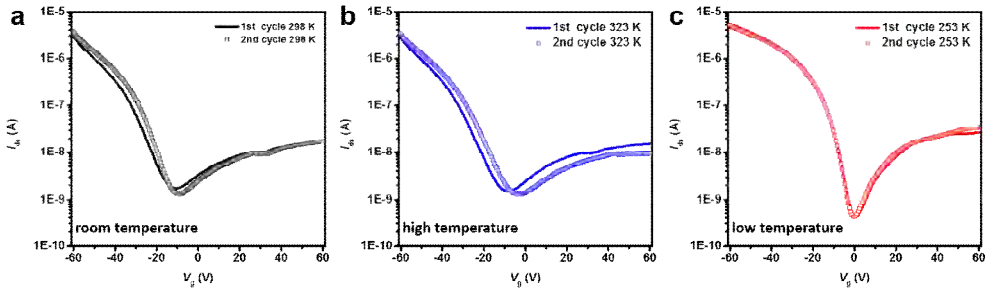

Figure S11. Current (logarithmic scale) to gate voltage curves obtained from a $BP_{Ag(+)}$ FET device under 253 K, 298 K and 323 K. The device was in turn stored at 298 K (room temperature), 253 K and 323 K for one day before its transport behavior was tested at the corresponding temperature. Then, another cycle of above experiment was taken on the same device.

Metal ions	Combine energy/ kcal
Ag	-41.8
Cu	-48.8
Li	-19.4
Na	-64.3
Mg	-75.1
Hg	-78.6

Figure S12. Combined energy of commonly used metal ions with BP calculated by DFT with the VASP package. Hundreds of phosphorus atoms are used to optimize the structure of BP and four typical consecutive phosphorus atoms are chosen as a supercell to simulate the interaction between BP and metal ions.

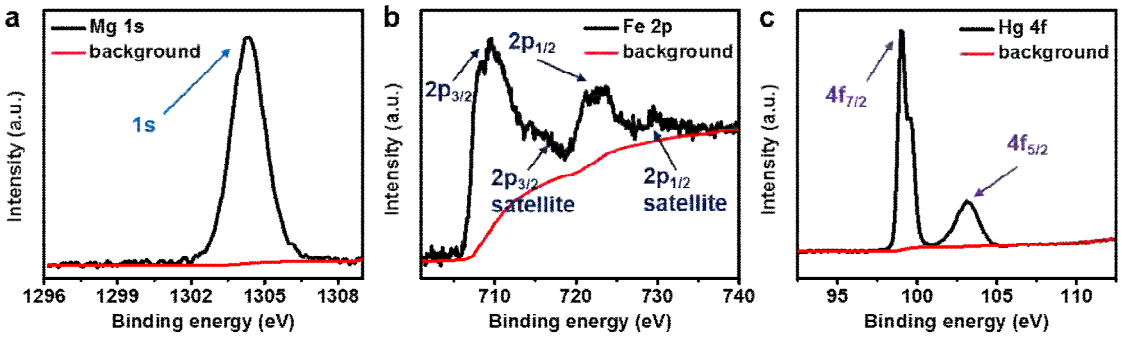

Figure S13. XPS spectra of (a) Mg 1s, (b) Fe 2p, and (c) Hg 4f on $BP_{Mg(2+)}$, $BP_{Fe(3+)}$, and $BP_{Hg(2+)}$, respectively.

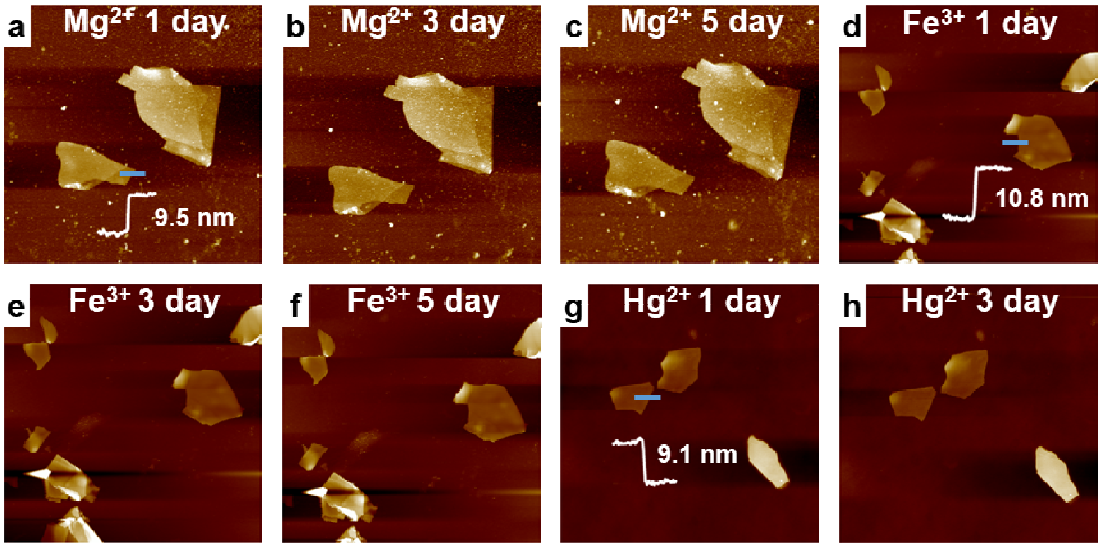

Figure S14. (a-c) AFM images of $BP_{Mg(2+)}$ sheets exposed to air for (a) 1 day, (b) 3 days, and (c) 5 days; (d-f) AFM images of $BP_{Fe(3+)}$ sheets exposed to air for (d) 1 day, (e) 3 days, and (f) 5 (f) days; (g-h) AFM images of $BP_{Hg(2+)}$ sheets exposed to air for (g) 1 day and (h) 3 days.

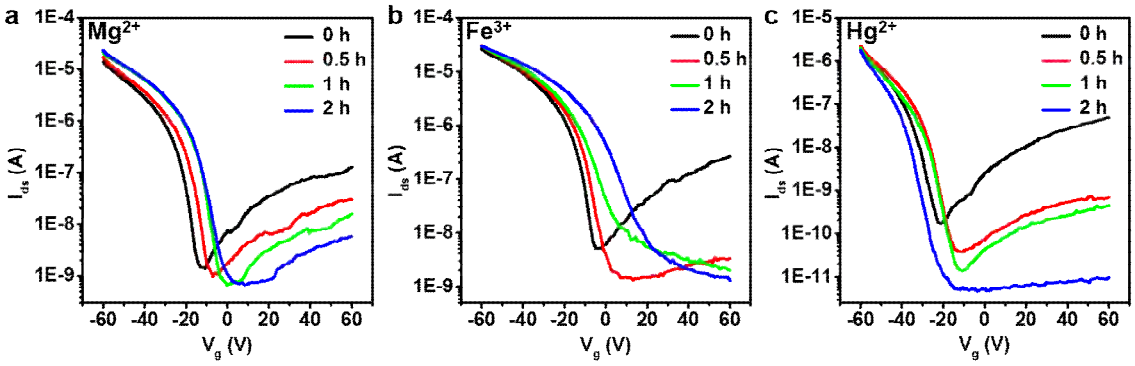

Figure S15. Current (logarithmic scale) to gate voltage curve obtained from the FET devices fabricated on BP sheets on silicon with 300 nm SiO_2 modified by (a) Mg^{2+}, (b) Fe^{3+}, and (c) Hg^{2+} at room temperature for different time.